applied sciences

MDPI

Article

An Experimental Study on the Sealing Mechanism of a Karst Pipeline by Dynamic Water Grouting

Jie Liu [1], Shuai Liu [2,*], Mingyuan Wang [2] and Bo Peng [2]

[1] Key Laboratory of Geological Hazards on Three Gorges Reservoir Area, Ministry of Education, China Three Gorges University, Yichang 443002, China; liujiea@126.com
[2] College of Civil Engineering and Architecture, China Three Gorges University, Yichang 443002, China; 15971634412@163.com (M.W.); 15274423796@163.com (B.P.)
* Correspondence: 15090139682@163.com

Abstract: Aiming at the problem of water burst plugging in karst pipelines, in this paper, a new type of waterborne epoxy resin magnetic self-polymerization grouting material (WEMS) suitable for karst pipeline water burst plugging was developed, and a visual simulation test device for karst pipeline water burst grouting plugging was designed and built. Through the orthogonal test of grouting plugging, the influence of different factors on the effect of grouting plugging was analyzed, and the shear mechanism of magnetic slurry magnetization plugging was also analyzed. The results showed that (i) the best grouting sealing performance was achieved when the new WEMS had a water–cement ratio of 0.35–0.55 and Fe_3O_4 powder misery of 20–40%. (ii) The primary relationship between the factors affecting the dynamic water flow rate and slurry retention is Fe_3O_4 power ratio > plugging length > water–cement ratio. (iii) The relationship equation was established between the shear strength of magnetic self-polymerizing slurry and the magnetic field strength, blocking length, and slurry ratio.

Keywords: karst pipe; grouting sealing; simulation test; grouting material

check for updates

Citation: Liu, J.; Liu, S.; Wang, M.; Peng, B. An Experimental Study on the Sealing Mechanism of a Karst Pipeline by Dynamic Water Grouting. *Appl. Sci.* **2024**, *14*, 1381. https://doi.org/10.3390/app14041381

Academic Editor: José António Correia

Received: 12 January 2024
Revised: 29 January 2024
Accepted: 30 January 2024
Published: 8 February 2024

Copyright: © 2024 by the authors. Licensee MDPI, Basel, Switzerland. This article is an open access article distributed under the terms and conditions of the Creative Commons Attribution (CC BY) license (https://creativecommons.org/licenses/by/4.0/).

1. Introduction

China's engineering construction industry is undergoing rapid development. The country is building infrastructure such as hydropower and water conservation, tunnels, mining, highways, bridges, subways, and other projects in high demand. These underground projects frequently involve engineering sudden water, gushing water, seepage, and other water hazards, which, if not handled properly or in a timely manner, can easily result in poor construction quality, slow progress, financial losses, and other issues. Surge water has become one of the most common geology dangers in tunnel and subterranean construction [1–4]. The most common and successful method of dealing with surge water disasters is grouting [5,6]. Many scholars have conducted extensive research on the theory and technology of grouting in water-rich and weak peripheral rocks, fault fracture zones, and so on, yielding numerous valuable scientific research results [7–9]. However, karst, the most widely distributed and largest area in China, has not been adequately researched in terms of the theory and method of its grouting treatment. As one of the main types of water influx in karst areas, karst pipe-type influx is characterized by a high flow rate and high velocity, ss depicted in Figure 1. At present, there are few studies on the mechanism and method of water gushing in karst pipes at home and abroad, so it is of great significance and engineering application value to study the mechanism and method of water gushing in karst pipes.

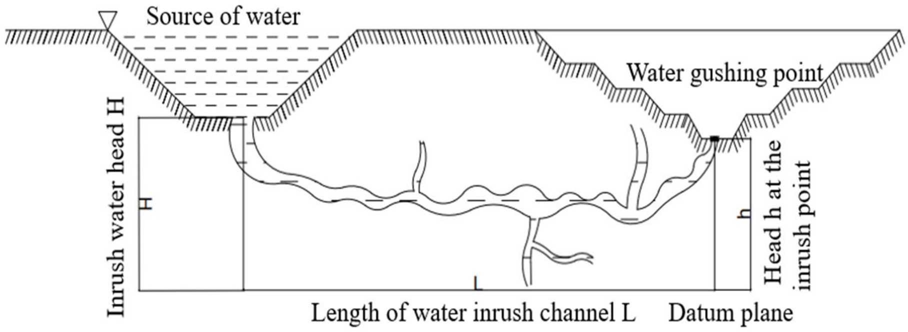

Figure 1. Typical hydraulic model of karst gushing water.

Traditional grouting materials have proven challenging to suit the needs of high-pressure, high-flow surge water projects, so developing new dynamic water grouting plugging materials has become a significant priority. Under dynamic water conditions, typical cement slurry is quickly diluted and scattered, and it cannot serve the job of a surge water sealer. Chemical slurry has been widely employed in gushing water control projects in recent years due to its benefits, which include resistance to dispersion under dynamic water circumstances, short setting time, high early strength, and superior profitability [10–12]. However, the general application of chemical grouting in the project may be limited by its potential for toxicity, environmental damage, high expense, etc. Thus, research into ways to increase grouting material retention rates, scour resistance, and ecologically friendly grouting material development in a dynamic water environment is crucial.

At present, many scholars at home and abroad have conducted a lot of research on the aspect of grouting and sealing of fissured rock and soil, while achieving more results. Bezuijen et al. [13] developed an analytical model depicting the fissure grouting test in sand. Sui et al. [14] carried out an experimental study on the closure effect of chemical grouting in rock fractures under dynamic water conditions. Liu and Sun [15] developed a grouting simulator based on the principle of parallel modeling to simulate grout flow in fractures. Xu et al. [16] developed a full-size physical model for simulation studies of high-pressure fracture grouting in rocks deep underground. Huang et al. [17] established an infiltration grouting model based on Maag's formula by taking the capillary force into account and proposed improved spherical and columnar grout diffusion formulas. Yang et al. [18] investigated the theoretical model of slurry diffusion on the basis of the existing generalized Darcy's law and derived an infiltration diffusion radius formula for power-law type slurry in sandy soil formations. Sui et al. [19,20] established a single-fissure flat plate model and conducted orthogonal tests to clarify the sealing mechanism of grouted slurry under dynamic water conditions. Li et al. [21] proposed the applicable range of their grouting materials by studying the characteristic law of viscosity change with the time of quick-setting type grouting materials under dynamic water conditions. However, there are fewer studies on the theory and method of grouting and sealing of large flow and high flow rate karst pipe-type gushing water, so it is of great significance to carry out research related to this for engineering applications.

Magnetorheological fluid is a new type of smart material. The concept of magnetorheological fluid was first proposed by Rabinow in the 1940s [22]. A magnetorheological (Mr) is a special material that can rapidly transform from a liquid phase to solid phase under the induction of an external magnetic field, which is called the Mr Effect [23]. Magnetorheological fluids are widely used, mainly in damping and damping, machinery, aerospace, and medical fields [24]. In the past decades, the study of the effect of magnetic fields on the mechanical properties of concrete materials in engineering has aroused great interest among researchers [25,26]. Ghorbani et al. [27] investigated the effect of magnetized mixing water on the densification of concrete with different fiber tragics through experiments. TaeseoKu [28] investigated the law of nanoparticles on the performance of grouting under water-rich conditions, and the results showed that the application of nanoparticles can effectively improve grout reinforcement performance. Mu et al. [29,30] used the piezomagnetic effect to study the force–magnetism relationship modeling at the interface of steel bars and reinforced concrete. Zhao et al. [31,32] miserably introduced magnetized water into concrete and found that the properties were greatly improved. Some scholars mixed magnetized steel fibers into concrete for magnetically induced orientation, which greatly enhanced the shear strength and flexural stiffness of the weak regions of the building. Liu et al. [33] utilized the attraction of ring magnets to magnetic materials, together with high-strength adhesives, to solve the leakage problem of diameter pipes. Liu et al. [34] proposed a new magnetic anchoring system with Fe_3O_4 powder as anchoring material and a magnetic metal rod as an anchoring rod, designed the mix ratio of artificial reef limestone, and determined the parameters of the magnetic anchoring system through orthogonal tests.

Based on the idea of the magnetorheological effect, this paper proposes a composite grouting material modified with Fe_3O_4 powder, which utilizes the magnetic field generated by a strong magnetic bar to make the slurry have a magnetic convergence effect, as shown in Figure 2, to improve the erosion resistance, retention rate, and shear resistance of the slurry, which can better achieve the effect of a grouting seal. Moreover, the self-developed visualization of a karst pipeline water gushing grouting plugging simulation test system, through the orthogonal test, can be used to explore the water–cement ratio, Fe_3O_4 powder tragedy, and the plugging length of the effect of the grouting plugging effect of the influence of the law, and also the formulae derivation of the magnetic slurry magnetization plugging shear resistance mechanism analysis. The study of the rule of WEMS grouting plugging under the condition of high dynamic water velocity can provide guidance for disaster prevention and mitigation of grouting plugging projects in the future.

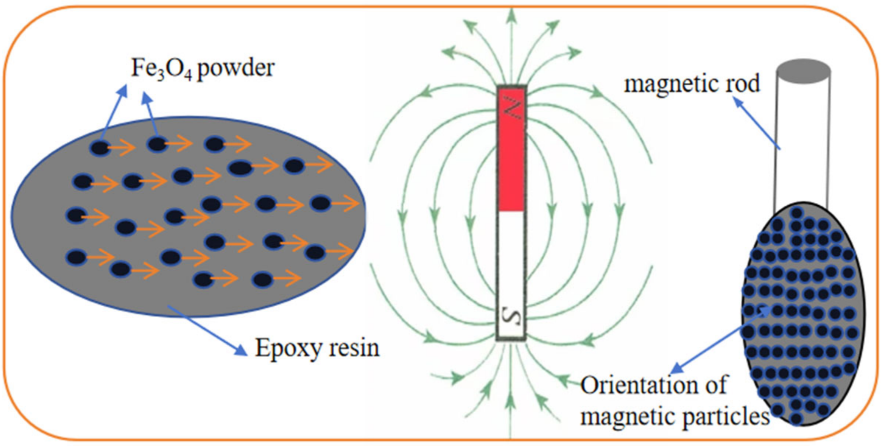

Figure 2. Diagram of the autoaggregation capacity of the slurry.

2. Pilot Study on WEMS

2.1. Experimental Materials

WEMS is a modified material of waterborne epoxy resin, mainly composed of water, cement, slurry material, Fe_3O_4, flocculant, and a water reducer, as shown in Figure 3. WEMS performance indicators require that the initial setting time is not earlier than 45 min, the final setting time is not later than 600 min, the fluidity is not less than 180 mm, the 28-day compressive strength is greater than 15 Mpa, and the quality of the construction material is the best at 25 °C.

Figure 3. Laboratory material.

2.1.1. Waterborne Epoxy Resin and Curing Agent

The slurry material is water-based epoxy resin; it belongs to the water-repellent material and consists of epoxy resin emulsion and curing agent. For the DY-56 water-based epoxy resin emulsion, a Dongyan water-based epoxy resin emulsifier is a kind of fast emulsification of an epoxy resin emulsifier, consisting of epoxy-based polyether with bicarbonate surfactant. For the DY175 water-based epoxy resin curing agent, the curing agent can be a completely water as a diluent and does not contain alcohol ethers or co-solvents. It can be used with a high molecular weight epoxy resin emulsion.

2.1.2. Nanoscale Magnetic Powders

The nanospherical Fe_3O_4 powder contains 99% Fe_3O_4 magnetic powder, which is magnetic and can move in a directional arrangement under the action of a magnetic field, with an average particle size of 80 nm~20 µm, a purity of 99.9%, a bulk density of 5.18 g/cm^3, a specific surface area of 50 m^2/g, and a color of black. Its chemical properties are stable and widely used.

2.1.3. Cement

The cement used was PO42.5 ordinary silicate cement produced by Hubei Huaxin Cement Co. (Wuhan, China). The main chemical components and performance indexes of the cement are shown in Table 1.

Table 1. Compositional analysis of ordinary silicate cement.

Component	SiO_2	Al_2O_3	Fe_2O_3	CaO	MgO	K_2O	SO_3	Loss
Content%	22.34	6.03	2.76	56.98	1.86	0.73	2.78	3.76

2.1.4. Flocculants

The concrete flocculant produced by Joynanda Specialty Materials Company (Shanghai, China) only used in this test has the advantages of good anti-dispersion, mobility, and a low segregation rate, reducing the loss of cement, etc., and at the same time, it has the advantages of no water seepage, controllable coagulation time, seepage resistance of up to S20 or more, and a corrosion resistance coefficient of not less than 0.85.

2.1.5. Water-Reducing Agents

The water-reducing agent selected for this test was produced by Hunan Xiangtan Homeland Building Materials Co, Ltd., Xiangtan, China, with the appearance of free-flowing powder, a bulk density of 500–700 g/L, active ingredient >90%, and a PH value between 6.0 and 9.0. It has the advantages of improving the plasticity and fluidity of concrete, reducing the water–cement ratio, mediating the setting time, and improving the strength and durability of concrete.

2.2. Test Program

When on-site grouting for water plugging and sealing, the fluidity, setting time, and early strength of the grouting material are the keys to sealing quality. However, the shear resistance of the grout will also have a large impact on the anti-seepage sealing effect, so in order to quantitatively describe the adsorption self-polymerization ability of the grout under the magnetic field strength, a closed-loop magnetic field adsorption range study is carried out. In this paper, the effects of different Fe_3O_4 powder dosages and water–cement ratios on the fluidity, adsorption range, setting time, and early strength of the grouting material are investigated, and a reliable new material of modified epoxy resin cement-based grouting is developed to support the on-site sealing construction.

In each set of tests, 0.8% water reducer and 7% flocculant were added to the cement paste, water–cement ratios were designed to be 0.35, 0.45, and 0.55, and the proportions of Fe_3O_4 powder were 20%, 30%, and 40%. The proportion of Fe_3O_4 powder was the proportion of the mass of cement. A total of nine groups of tests were designed, and the proportion parameters for each group are shown in Table 2. The flowability, setting time, adsorption range, and compressive strength of each group were tested during the tests.

Table 2. Test proportioning parameters.

Serial Number	Cement/g	Water/g	Epoxy Resin/g	Curing Agent/g	Fe_3O_4 Powder/%	Flocculants/%	Water Reducer/%
1	100	35	12	10.2	20	7	0.8
2	100	35	12	10.2	30	7	0.8
3	100	35	12	10.2	40	7	0.8
4	100	45	12	10.2	20	7	0.8
5	100	45	12	10.2	30	7	0.8
6	100	45	12	10.2	40	7	0.8
7	100	55	12	10.2	20	7	0.8
8	100	55	12	10.2	30	7	0.8
9	100	55	12	10.2	40	7	0.8

2.3. Test Methods

2.3.1. Liquidity Testing

In this paper, according to the polymer-modified cement mortar test method, the flowability test was carried out using the flow mold of cement net slurry to characterize its flowability performance. The diameter of the upper mouth of the flow mold is 36 mm, the diameter of the lower end is 60 mm, the height is 60 mm, and the wall thickness is about 2–3 mm. The prepared slurry is put into the truncated cone circular mold, scraped flat with a spatula, and then immediately lifting the truncated cone circular mold vertically upward. Gently wait for the slurry to flow on a glass plate for 120 s and then use a straightedge to measure the flow distance of the slurry flow in the transverse and longitudinal directions. The average value of the slurry flow is taken as the fluidity degree, which is shown in Figure 4a.

Figure 4. Material performance test.

2.3.2. Compressive Strength Test

The slurry was poured into test molds 50 mm × 100 mm in size according to the cement strength test standards. It was cured under natural curing strips for 7, 14, and 28 days. The cement strength test was conducted according to the "Cement Mortar Strength Test Method", and the test was conducted using an RMT-150C Rock Mechanics Test System, adopting the force-displacement loading method and testing WEMS, as shown in Figure 4b.

2.3.3. Adsorption Range Testing of Grouting Materials

In order to evaluate the adsorption range of magnetic slurry, the adsorption diameter (d) index was used in this study. First, a mixture totaling 1.5 L of grout material was prepared and placed into a 2 L beaker. Second, a magnetic bar with a diameter of 20 mm and a magnetic field strength of 12,000 GS was inserted into the center of the beaker, adsorbed for 30 s, and then removed. The adsorption diameter was measured with a straightedge, as shown in Figure 4c.

2.3.4. Setting Time Test

The test method for the setting time of a polymer-modified mortar is designed according to the standard DL/T5126-2001 [35] test procedure for a polymer-modified cement mortar [35]. Prepare the slurry according to the selected ratio, inject the prepared slurry directly into the circular mold (without vibration), scrape it off, and immediately put it under the initial (final) setting needle of the Vicat meter, and test it once every half hour interval, rotate the nut on the Vicat meter, read the number shown in the Vicat meter, i.e., the initial (final) setting needle penetration, and judge whether the slurry achieves the initial (final) setting, as shown in Figure 4d.

2.4. Experimental Results

Based on the above scale experiment, the experimental data statistics are shown in Table 3.

Table 3. Test data statistics.

Number	Fluidity/mm	Initial Setting Time/min	Final Setting Time/min	Adsorption Range/mm	Compressive Strength/MPa		
					7 d	14 d	28 d
1	199.5	95.00	170.00	10.50	12.00	16.40	20.10
2	189.0	129.00	186.00	12.50	14.70	21.50	26.10
3	178.0	164.00	220.00	14.00	18.30	29.40	34.30
4	209.5	122.00	186.00	9.50	8.20	13.65	17.80
5	194.5	156.00	212.00	10.50	10.60	20.80	25.30
6	189.0	196.00	262.00	12.00	13.60	24.70	30.20
7	232.5	260.00	376.00	8.00	3.30	10.20	12.60
8	215.0	326.00	442.00	9.50	5.30	13.40	16.30
9	202.0	428.00	546.00	11.00	9.60	21.50	24.40

2.4.1. Liquidity Analysis

Due to the small particle size of the magnetic slurry, the material can enter into the tiny cracks to achieve the best repair effect. In order to better study the fluidity of the slurry, quantitative analysis was carried out to analyze the fluidity performance of the slurry under the effect of different ratios. As can be seen in Figure 5, with the increase in the water–cement ratio, the magnetic self-polymerization slurry fluidity significantly improved, while in the water–cement ratio of the same conditions, the Fe_3O_4 powder had a tragic amount of impact on the fluidity of the negative correlation, i.e., the larger the ratio, the lower the slurry fluidity. Relative to the magnetic slurry water–cement ratio of 0.35 and magnetic slurry water ratio of 0.45 to 0.55, the fluidity increased by 5% to 17.9%, respectively. The main reason is the increase in the water–cement ratio will increase the water content in the cement slurry and increase the wetting and dispersion of cementitious sand so that the friction between the particles is reduced, thus improving flow fluidity. Due to the small particle size of the magnetic slurry, the material can enter into the tiny cracks to achieve the best repair effect. In order to better study the fluidity of the slurry, quantitative analysis was carried out to analyze the fluidity performance of the slurry under the effect of different ratios. As can be seen in Figure 5, with the increase in the water–cement ratio, the magnetic self-polymerization slurry fluidity significantly improved, while in the water–cement ratio of the same conditions, the Fe_3O_4 powder had a tragic amount of impact on the fluidity of the negative correlation, i.e., the larger the ratio, the lower the slurry fluidity. Relative to the magnetic slurry water–cement ratio of 0.35 and magnetic slurry water ratio of 0.45 to 0.55, the fluidity increased by 5% to 17.9%, respectively. The main reason is that the increase in the water–cement ratio will increase the water content in the cement slurry and increase the wetting and dispersion of cementitious sand so that the friction between the particles is reduced, thus improving flow fluidity.

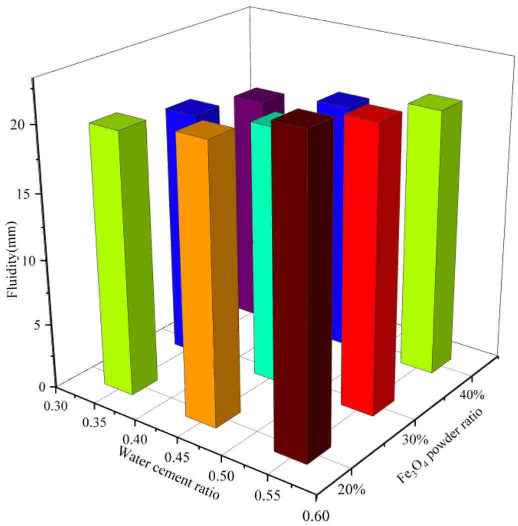

Figure 5. Liquidity test results.

2.4.2. Adsorption Range Analysis

As can be seen in Figure 6, with the increase in magnetic slurry water–cement ratio, the magnetic bar adsorption range gradually decreased; when the magnetic slurry water–cement ratio is certain, with the gradual increase in Fe_3O_4 powder doping, the magnetic bar adsorption diameter gradually increased; that is, the greater the slurry's self-polymerization ability. This is because ① with the increase in the water–cement ratio, the slurry internal water content increases so that in the magnetic field strength attraction, the slurry of the internal friction angle decreases; the magnetic particles are adsorbed very quickly with the other material segregation, and epoxy resin on the magnetic particles of the wrapping is greatly reduced, so that the adsorption capacity is weakened; therefore, with the increase in the water–cement ratio, the diameter of adsorption becomes smaller and smaller. ② Magnetic particles in the slurry by the magnetic field will be arranged in accordance with the direction of the magnetic induction line to form a magnetic chain; with the increase in Fe_3O_4 doping, the density of the magnetic particles in the slurry becomes larger, the formation of the magnetic chain will become longer so that it can more tightly adhere to the magnetic rod around the slurry viscosity increases, the angle of internal friction becomes larger, and, therefore, with the increase in the doping amount of Fe_3O_4, the larger the diameter of the adsorption.

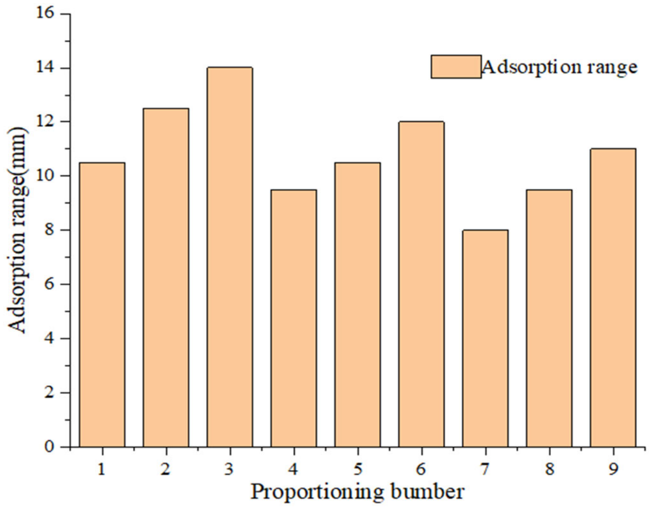

Figure 6. Adsorption range result.

At the same time, the increase in magnetic field strength makes the adsorption diameter increase. As the magnetic particles are in the slurry under the action of the magnetic field, they form a strong adsorption, while the water-based epoxy resin, cement and magnetic particles wrap each other, increasing the internal friction Angle and cohesion of the slurry, and the agglomeration effect is more obvious, so the magnetic self-polymerizing slurry has a certain shear resistance under the condition of dynamic water.

2.4.3. Setting Time Analysis

In Figure 7, it can be seen that the shortest initial setting time of WEMS is 95 min, the longest initial setting time is 428 min, the shortest final setting time is 170 min, and the longest final setting time is 546 min. The water–cement ratio significantly prolongs the setting time. With the increase in the water–cement ratio, the initial setting time and final setting time of the slurry gradually increased. Under the same water–cement ratio, the initial and final setting time of the slurry increased with the increase in Fe_3O_4 powder dosage. When the water–cement ratio is 0.55 when the dosage is increased from 20% to 40%, the initial setting time is increased from 260 min to 428 min, and the final setting time is increased from 376 min to 546 min, and the dosage of Fe_3O_4 powder has an obvious retardation effect on the slurry. The main reason is that after adding Fe_3O_4 powder in the slurry, Fe_3O_4 powder with a small particle size forms a small parcel on the surface of cement particles, which separates the contact area of cement particles and water to a certain extent, prevents the coagulation of cement particles, inhibits further hydration reaction of the cement, and delays the coagulation of the cement, but the interval between the initial setting time and the final setting time varies greatly throughout the stage.

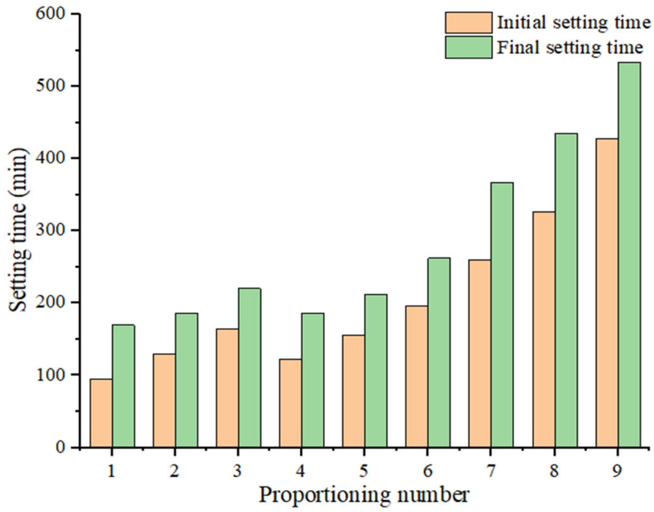

Figure 7. Setting time test results.

2.4.4. Compressive Strength Analysis

As can be seen in Figure 8, when the amount of Fe_3O_4 powder tragedy is certain, with the increase in the water–cement ratio, the uniaxial compressive strength of the material shows a decreasing trend. Keeping the water–cement ratio of the material unchanged, when the amount of Fe_3O_4 powder tragedy is changed, the compressive strength of the material is positively correlated with the amount of Fe_3O_4 powder tragedy. The main reason is with the increase in the water–cement ratio in the material, the hydration reaction of cement requires too much water, resulting in the existence of hardened microporosity within the material; this microporosity is due to the evaporation of water molecules retained, which will lead to the strength of the lower being larger. As the micron-sized Fe_3O_4 powder itself has strong strength, the slurry can fill the tiny pores caused by water evaporation due to the hydration reaction but does not participate in the reaction in the middle of the role of a certain skeleton, so it will improve the strength of the material when the water–cement ratio of 0.35, the Fe_3O_4 powder miserable amount of 40%, and the material compressive strength reach their maximum values. The material basically reaches more than 80% of its strength at the age of 14 days, and the growth rate from 14 to 28 days is less than 10%, so the material basically forms its strength at the age of 14 days.

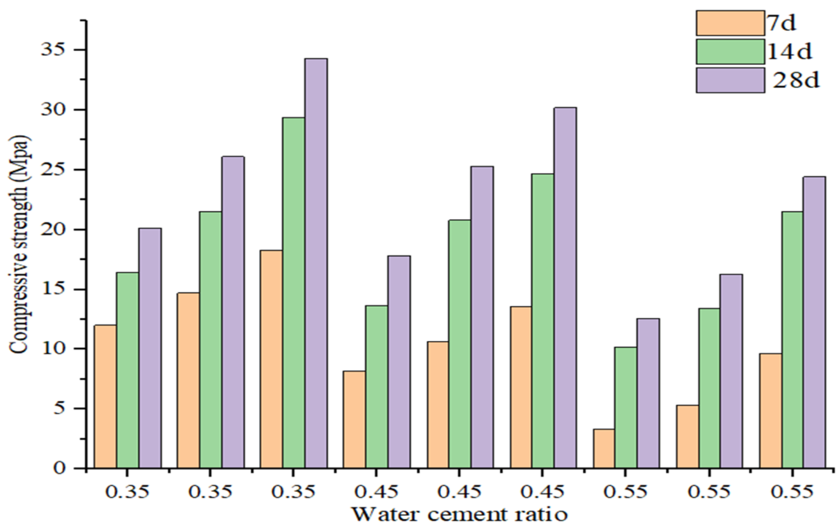

Figure 8. Compressive strength results.

Through the indoor proportion test, we analyzed the influence law of factors, such as the water–cement ratio and Fe_3O_4 powder tragic amount, on the basic properties of WEMS, such as fluidity, setting time, adsorption range, and compressive strength. Conclusion: With the increase in the water–cement ratio, the fluidity of magnetic self-polymerizing grout increases significantly, and the influence of Fe_3O_4 powder on the fluidity is negatively correlated with the constant water–cement ratio. The increase in the water–cement ratio inhibited the magnetic self-aggregation ability of the slurry, and the larger the Fe_3O_4 powder content, the larger the magnetic rod adsorption diameter; that is, the stronger the self-aggregation ability of the slurry. The water–cement ratio will significantly prolong the setting time of the material. The influence of the water–cement ratio on the uniaxial compressive strength of the material is negatively correlated, and the compressive strength of the material is positively correlated with the Fe_3O_4 powder content. All performance indicators of WEMS meet the requirements and determined the optimal mixing ratio of Fe_3O_4 powder to be 20–40%, which is an important guiding significance for the treatment of karst pipe water gushing grouting.

3. Dynamic Water Sealing Test Study

3.1. Experimental Systems

The visualization simulation test system of karst pipe water gushing grouting and plugging is developed by China Three Gorges University. The simulation test system, which is divided into five parts: a dynamic water simulation system, pipe visualization system, grouting control system, magnetic field generation system, and data acquisition system, is shown in Figure 9. Through a series of grouting tests, the influence of factors, such as the water–cement ratio of the material, the tragic amount of Fe_3O_4 powder, and the blocking length on the effect of grouting blocking, is analyzed.

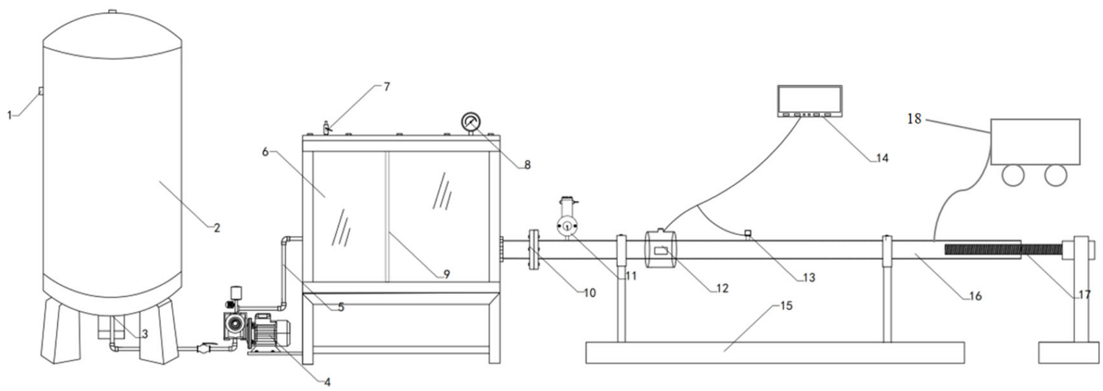

As shown in the figure: 1.Water inlet 2.Water tower 3.Water outlet 4.Pressure pump 5.Pressurized inlet pipe 6.Organic glass pressure water storage tank 7.Exhaust valve 8.Pressure gauge 9.Water rectifier plate 10.Organic glass flange plate 11.Flow control valve 12.Turbine flow meter 13.Pressure sensotr 14.Paperless recorder 15.Pipe holder 16.Acrylic tube 17.Magnetic rod 18.Grouting system

Figure 9. Self-developed grouting plugging simulation experiment system.

The pipe vision system consists of a 50 mm pipe diameter visual pipe and a pipe bracket made of acrylic material (Figure 10). Acrylic is a chemical material with the chemical name polymethyl methacrylate, which is a lightweight, rugged, transparent, and easy-to-work-with material. To ensure visibility, the single pipes are connected by acrylic flanges and, through steel supports, erected on the ground.

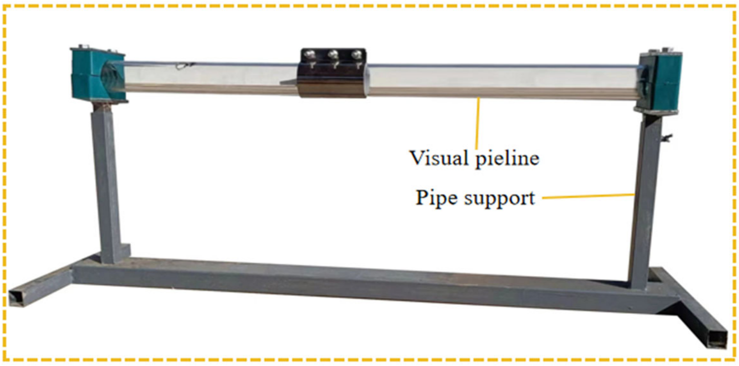

Figure 10. Visual piping system.

The dynamic water simulation system comprises a water storage tank, a water pump, and a Plexiglas pressure storage tank. At the front end of the pipe inlet and volume of 0.125 m^3 (0.5 m × 0.5 m × 0.5 m), the plexiglass water storage tank is connected to ensure the stability of the given head. In contrast, the other end of the plexiglass water storage tank is connected to the pump, increasing the pressure of the water body in the tank. The flow rate measuring instrument and pressure sensing are set on the piping system to monitor the dynamic water in the pipeline. The central monitoring items are water pressure and water velocity, and the results are imported into the paperless recorder. The recording interval is 1 s, and the component parameters of the data acquisition equipment are shown in Table 4.

Table 4. Various data acquisition equipment parameters.

Name	Paperless Recorder	Electrical Flowmeter	Pressure Pickup
Model	SIN-R9600	LD-DN25	BX-131
Range	−999~R9600	1.2–12 m^3/h	0–1 MPa
Precision	0.3%	0.5%	0.5%
Output signal	4–20 mA	4–20 mA	4–20 mA
Measuring medium	Water, slurry, oil	Water, slurry, oil	Water, slurry, oil

3.2. Experimental Scheme

In the magnetic slurry plugging material used in this paper, under the adsorption effect of magnetic field strength, the viscosity of slurry increases with the increase in magnetic field strength; its fluidity decreases and the slurry consistency increases, showing the characteristics of non-Newtonian fluid and reverse thixotropy. Insert the magnetic flux of 14,000 GS and the diameter of a 30 mm magnetic bar at the outlet end of the pipeline system, and the test is based on the dynamic water flow rate of 0.2 m/s and the grouting pressure of 0.3 MPa to change the parameters of the water–cement ratio, the Fe_3O_4 powder doping ratio, and the blocking length to carry out the orthogonal test. The sealing effect of WEMS on the water gushing in the karst pipeline was evaluated according to the change in water pressure in the pipeline, the change in water flow rate, and the retention rate of the slurry. The factor level table and the theoretical design of the orthogonal experiment are shown in Tables 5 and 6, respectively.

Table 5. Horizontal factor.

Factor Level	Slurry Type	Water Cement Ratio	Fe_3O_4 Power Ratio	Plugging Length (mm)
1	WEMS	0.35	20%	100
2		0.45	30%	200
3		0.55	40%	300

Table 6. Orthogonal experiment scheme design.

Test Number	Slurry Type	Water Cement Ratio	Fe_3O_4 Power Ratio	Plugging Length (mm)
1	WEMS	0.35	20%	100
2		0.35	30%	200
3		0.35	40%	300
4		0.45	20%	200
5		0.45	30%	300
6		0.45	40%	100
7		0.55	20%	300
8		0.55	30%	100
9		0.55	40%	200

3.3. Test Methods

The water plugging pressure, slurry retention rate, and dynamic water flow rate in the pipe were selected to evaluate the grouting blocking effect. The larger the water plugging pressure is, the better the magnetization plugging effect is. Under the condition of moving water, the larger the slurry retention rate is, the better the grouting blocking effect is. The more prominent the reduction in the dynamic water flow rate in the pipeline, the more significant the effect of grouting is directly indicated.

3.3.1. Monitoring Data Acquisition

The magnetized blocking pressure is obtained using a pressure transducer, and the dynamic water velocity in the pipe is read by a flow meter, as shown in Figure 11.

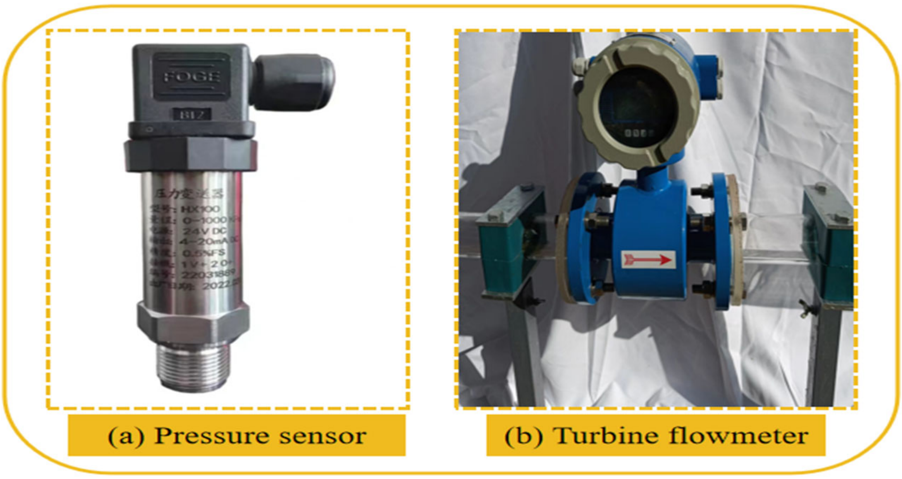

Figure 11. Monitoring device.

3.3.2. Slurry Retention Rate

First, the grouting material is configured and put on the electronic scale to weigh the total mass of the slurry and grouting irrigation W_1 after the grouting is completed in the grouting irrigation mass W_2. Before the test, weigh the total mass of the plexiglass tube and the magnetic bar as W_3. The water pump is used to simulate the dynamic water flow, the water retaining plate with a filter hole is used to maintain the uniform flow rate, and a filter is placed at the end to recover the grouting material washed away by the water. After the test was completed, the total mass W_4 of the plexiglass tube, the magnetic rod, and the grouting material were weighed. Under the condition of dynamic water, the percentage of slurry in the organic glass tube to the original slurry (hereinafter referred to as the retention rate) is compared, and the calculation formula of the retention amount is shown in Formula (1).

$$\text{Slurry retention rate} = \frac{W_4 - W_3}{W_1 - W_2} \times 100\% \quad (1)$$

3.4. Results and Discussion

Plugging Pressure Analysis

The magnitude of the slurry plugging pressure under dynamic water conditions responds to the effect of anti-seepage plugging. An intuitive analytical method was used to analyze the test data, revealing the primary and secondary relationships between the factors and the slurry plugging pressure. The analyzing steps are as follows:

(1) Calculate the sum of the test results under each factor condition, defined as k_{i};
(2) Take the average value of the above K_i, defined as k_i;
(3) Calculate the extreme difference R using the difference between max $\overline{k}_i$ and min $\overline{k}_i$ and determine the degree of influence of each factor on the test index by the R-value.

The experimental results are visually analyzed in the table, as shown in Table 7. Based on the above experimental data, it can be seen that the primary and secondary relationships of the factors affecting the effect of grouting sealing are plugging length > Fe_3O_4 power ratio > water–cement ratio. Each of the factors analyzed in Figure 12 has an obvious correlation with the water plugging pressure. The specific trends are as follows:

(1) With the increase in plugging length, the average pressure increased by 51.2% when the plugging length increased from 100 mm to 200 mm. When the plugging length increases from 200 mm to 300 mm, the average pressure increases by 29.7%. There is a significant positive correlation between plugging length and plugging pressure.
(2) As the water–cement ratio increases, the plugging pressure decreases. As the water–cement ratio increases, the solid phase concentration decreases, so the slurry's plastic viscosity and ultimate shear decrease, significantly reducing the contact force between the slurry and the pipeline, making the sealing effect of the slurry worse.
(3) The plugging pressure also increases with the increase in the amount of Fe_3O_4 powder tragedy. When Fe_3O_4 powder tragedy increases, the plastic viscosity of the magnetic slurry reduces, and under the action of the external magnetic field, the slurry's original loss of rheology viscosity will instantly increase, and the contact stress between the particles are used to enhance the angle of friction, thus making the magnetic slurry plugging shear capacity increase.

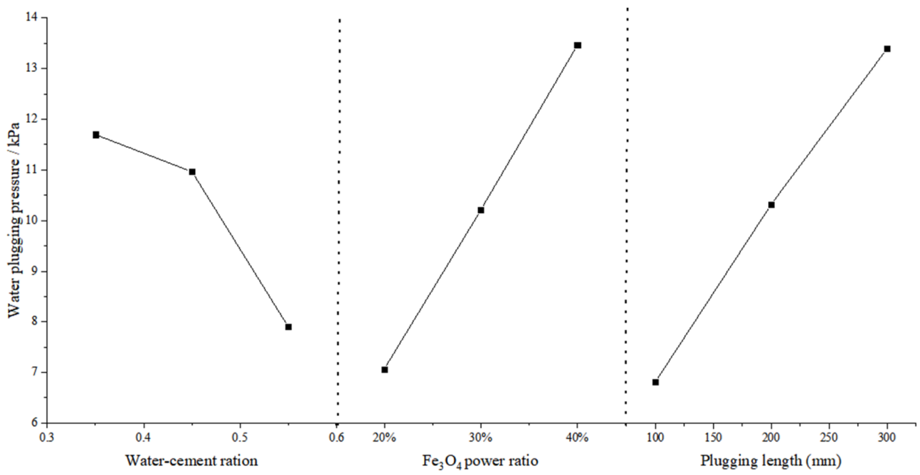

Figure 12. Influence of various factors on water plugging pressure.

Table 7. Intuitive water pug pressure analysis table.

Factor	Water–Cement Ratio	Fe_3O_4 Power Ratio	Plugging Length (mm)
K_1	35.10	23.40	20.50
K_2	32.90	30.50	31.00
K_3	23.70	37.80	40.20
k_1	11.70	7.800	6.83
k_2	10.96	10.17	10.33
k_3	7.900	12.60	13.40
Range	3.80	4.80	6.57
Primary and secondary factor	Plugging length > Fe_3O_4 power ratio > water–cement ratio		

3.5. Analysis of Velocity of Dynamic Water and Dynamic Water Scour Resistance Effects

In dynamic water grouting, dynamic water has a large scouring effect on the slurry adsorbed by the magnetic rod. By analyzing the scouring effect of moving water on the slurry, the influence of moving water on the slurry retention rate can be fully understood. Based on the above experimental data, polar analysis was used to determine the influence of the above factors on the two test indexes of velocity of dynamic water and slurry retention rate, and the results are shown in Tables 8 and 9.

Table 8. Intuitive velocity of dynamic water analysis table.

Factor	Water–Cement Ratio	Fe_3O_4 Power Ratio	Plugging Length (mm)
K_1	0.521	0.540	0.484
K_2	0.511	0.506	0.506
K_3	0.486	0.473	0.528
k_1	0.174	0.180	0.161
k_2	0.170	0.169	0.169
k_3	0.162	0.156	0.176
Range	0.012	0.022	0.015
Primary and secondary factor	Fe_3O_4 power ratio > plugging length > water–cement ratio		

Table 9. Intuitive hydrodynamic anti-erosion effect analysis table.

Factor	Water–Cement Ratio	Fe_3O_4 Power Ratio	Plugging Length (mm)
K_1	24.54	25.20	22.73
K_2	23.43	23.24	23.76
K_3	23.36	23.01	24.84
k_1	8.18	8.40	7.58
k_2	7.81	7.75	7.92
k_3	7.79	7.67	8.28
Range	0.39	0.73	0.70
Primary and secondary factor	Fe_3O_4 power ratio > plugging length > water–cement ratio		

As can be seen in Tables 8 and 9, in a pipe diameter of 50 mm, the velocity of dynamic water and the dynamic water scour resistance effect are most affected by the Fe_3O_4 misery, followed by the blocking length, and least affected by the water–cement ratio. Figures 13 and 14 show the effects of various factors on the velocity of dynamic water and dynamic water scour resistance.

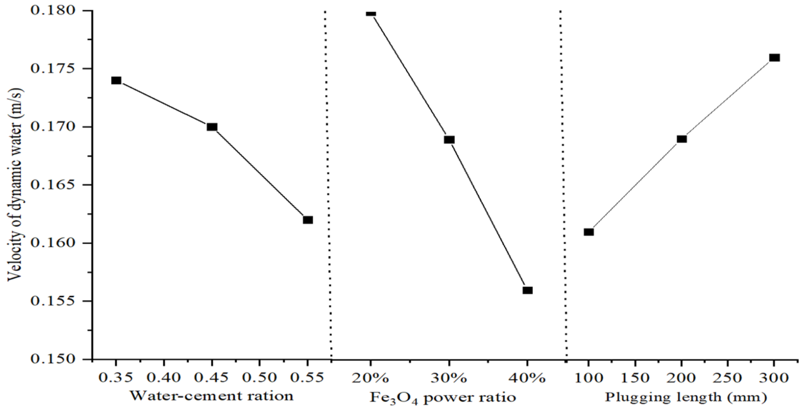

Figure 13. Influence of various factors on the velocity of moving water.

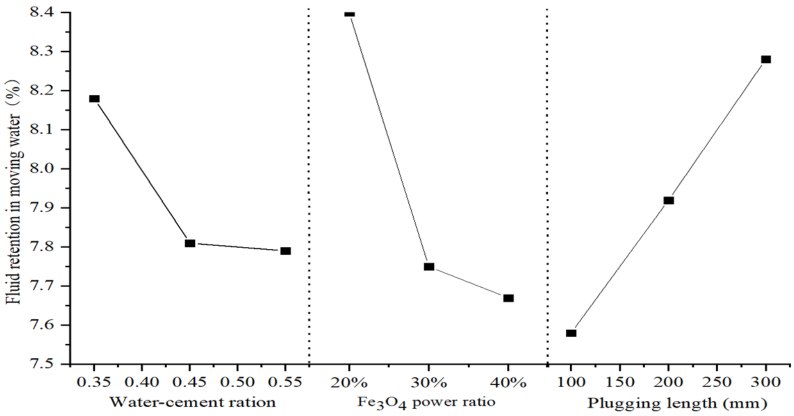

Figure 14. Influence of various factors on the retention rate of the slurry.

The trends of the factors affecting the flow rate of moving water and the effectiveness of moving water against scouring are as follows:

(1) The velocity of dynamic water and the dynamic water scour resistance effect negatively correlate with the water–cement ratio. The water–cement ratio of the slurry affects its specific gravity, dynamic viscosity, and rheological properties. The smaller the water–cement ratio, the larger the specific gravity and dynamic viscosity of the slurry and the poorer the fluidity, and the sassafras force between the slurry and the pipe wall becomes larger, so it makes the velocity of dynamic water decrease, and the slurry retention rate becomes larger.

(2) The velocity of dynamic water and dynamic water scouring resistance is negatively correlated with the amount of Fe_3O_4. As the amount of Fe_3O_4 increases, the number of magnetic powder particles wholly wrapped by the base liquid increases, and at the same time, under the effect of magnetic field magnetization, the instantaneous viscosity of the slurry increases and the contact force between the magnetic particles is enhanced, which means that the magnetic rod adsorption of the slurry attached to the body is also gradually increased; it not only enhances the slurry to the resistance of the water but also increases the slurry's dynamic water scouring resistance effect.

(3) The velocity of dynamic water and dynamic water scouring resistance effect positively correlate with the blocking length. Due to the increase in blocking length, the magnetic slurry adsorbed by the magnetic rod increases, so the slurry that impedes the water flow increases, the speed of the dynamic water scouring slurry slows down, and the slurry loss rate slows down so that the velocity of dynamic water decreases and the performance of the dynamic water scouring resistance enhances.

4. Analysis of the Shear-Resisting Mechanism of Magnetic Slurry Magnetized Blocking

4.1. Magnetic Field Magnetism Model

In order to quantitatively portray the mechanical mechanism of magnetic slurry sealing shear resistance, the magnetic induction lines of a specific section of the magnetic bar are set to be distributed as a ring, and the magnetic induction lines between the remaining sections have no superimposed influence on each other, constituting a closed-loop magnetic field, as shown in Figure 15.

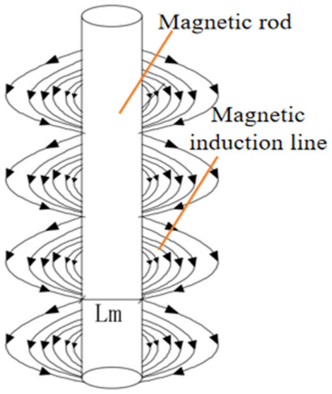

Figure 15. Magnetic induction line distribution.

Basic assumptions:

(1) It is assumed that the slurry is homogeneous and is in a state of fully saturated magnetization;
(2) It is assumed that the magnetic medium inside the magnet is homogeneous.

In accordance with Ampere's view on the molecular circulation of the magnetic field, the magnetic field vector in space is represented by the magnetic induction intensity. Let the coordinates of any point in space be P(x, y, z), and take the micrometric body to obtain its intensity as follows:

$$dB = \frac{\mu_0}{4\pi} \frac{Idl \times (r - r')}{|r - r'|^3} \tag{2}$$

r is the vectorial diameter at a point and μ_0 is the magnetic permeability.

Thus, the magnetic susceptibility generated at a point is

$$B = \frac{\mu_0}{4\pi} \int_0^l \frac{Idl \times (r - r')}{|r - r'|^3} \tag{3}$$

Therefore, the magnetic field strength is

$$M = \frac{B}{\mu_0} - \frac{\sum \mathrm{m}}{\Delta V} \tag{4}$$

where m denotes the magnetic moment of a single cell.

When the material is outside the permanent magnet, i.e., when the magnetization strength, $M = 0$. The magnetic field strength is calculated as follows:

$$H = \frac{B}{\mu_0} \tag{5}$$

The magnetic rods used in the test are cylindrical magnetic rods. Set the magnetic field origin of the magnetic rods coordinates for $P_0(x_0, y_0, z_0)$, the magnetic induction line range of a point with the coordinates of $P_1(x_1, y_1, z_1)$, and then the magnetization density J_s and the relationship between the magnetization strength n for $J_S = M \times n$. Next, take the radius of the cylindrical magnet for the magnetic field ring, and then the total magnetic field at a certain point is as follows:

$$B = B_x i + B_y j + B_z k = \int_0^r dB_x i + dB_y j + dB_z k \tag{6}$$

4.2. Derivation of Shear Strength Equations for Magnetic Slurries

As can be seen from the distribution law of magnetic induction lines, a larger magnetic field is formed around the magnetic bar so that the magnetically converging slurry is closely adsorbed on the magnetic bar, as shown in Figure 16a, which greatly improves the blocking anti-shear capacity. In order to quantitatively analyze the change rule of the magnetic field in space, the magnetic field strength at different distances from the magnetic bar was measured with a Gauss meter, and the formula was fitted, as shown in Figure 17.

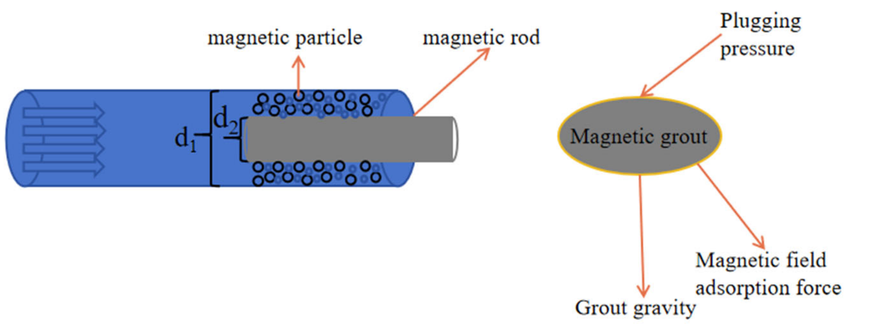

(a) Plugging diagram (b) Magnetic grout force diagram

Figure 16. Force diagram of magnetic particles.

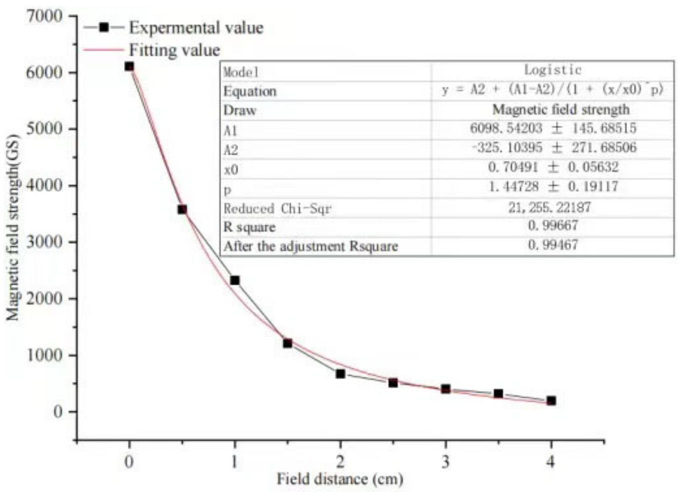

Model	Logistic
Equation	y = A2 + (A1-A2)/(1 + (x/x0)^p)
Draw	Magnetic field strength
A1	6098. 54203 ± 145. 68515
A2	-325. 10395 ± 271. 68506
x0	0. 70491 ± 0. 05632
p	1. 44728 ± 0. 19117
Reduced Chi-Sqr	21, 255. 22187
R square	0. 99667
After the adjustment Rsquare	0. 99467

Figure 17. The magnetic field strength at different distances.

The fitting formula is

$$y = \frac{6334}{1 + (x/0.704)^{1.44}} + 325 \tag{7}$$

where x is the magnetic field distance and y is the magnetic field strength.

When the plugging reaches the peak value, a critical failure is about to occur. The slurry plugging is affected by several forces, namely, the water plugging pressure, the adsorption force of the slurry affected by the magnetic field, and the gravity of the slurry itself. Figure 16b shows that the damage of the slurry is a shear failure. When the plugging pressure reaches the peak value, that is, the combined force of the adsorption force of the slurry and the gravity of the slurry itself is equal to the peak value of the plugging pressure, which is as follows:

$$F_F = F_G + F_\mu = \rho_f g \tag{8}$$

In the formula, F_F is the plugging pressure, F_G is the magnetic field strength at different distances, and F_μ is the gravity of the slurry.

The shear strength is as follows:

$$\tau = \frac{F}{A} = \frac{F_G + F_\mu}{A} \tag{9}$$

In the formula, A refers to the shear force area affected by the adsorption diameter. Because the shear force in the test is circumferential, that is, equivalent to the plane uniform force, the average shear strength is as follows:

$$\tau = \frac{F}{A} = \frac{F}{RH} \tag{10}$$

In the formula, R is the whole adsorption diameter, including the magnetic field diameter, and H is the length of the stress surface.

Substituting the above formula into the space total magnetic field calculation Formula (6), we obtain the following:

$$H = k[-\psi(r-y, r-x, z) - \psi(r-x, r-z, y) - \psi(r-y, r-z, x) - \psi(x, y, z)] \tag{11}$$

In the formula, $k = \frac{J_s}{4\pi} = \frac{M \times n}{4\pi}$, that is, $H = H(r, h, J_S)$, and because $J_S = M \times n$

$$J_S = \left(\frac{6334}{1 + (x/0.704)^{1.44}} + 325\right) \times M = \left(\frac{6334}{1 + (x/0.704)^{1.44}} + 325\right) \times 4 \tag{12}$$

In the plugging test, the magnetic slurry is directly adsorbed on the magnetic rod and is adsorbed by the longitudinal magnetic force from the magnetic rod to form shear resistance. Therefore, only the magnetic field intensity in the Z direction is considered in the calculation.

$$H_Z = \frac{\left(\frac{6334}{1+(x/0.704)^{1.44}} + L\right)}{4\pi}[-\psi(4,4,z) - \psi(0,4,z) - \psi(4,0,z) - \psi(0,0,z) - \psi(4,4,z-1.5)] \tag{13}$$

The above shear strength calculation formula is brought in, and the peak shear strength H_Z of the magnetic slurry is as follows:

$$H_Z = \frac{\left(\frac{6334}{1+(L/0.704)^{1.44}} + 325\right)^2 \times L}{4\pi}\tau = \frac{\left(\frac{6334}{1+(L/0.704)^{1.44}} + 325\right)^2 \times L}{4\pi} \times \frac{F}{LH} \tag{14}$$

In the formula, L is the magnetic field distance, H is the length of the stress surface, and F is the plugging pressure.

The shear strength of the magnetic slurry under different water plugging lengths was obtained by selecting a water–cement ratio of 0.35 and a water plugging pressure of 20%, 30%, and 40% of Fe_3O_4 powder, as shown in Table 10.

Table 10. Weak anti-shear parameters of magnetic grout under different plugging lengths.

Magnetic Field Strength	14,000 GS		
Fe_3O_4 power ratio	20%	30%	40%
Plugging length (mm)	100	200	300
Water plugging pressure (kPa)	6	11.4	17.7
Shear strength (kPa)	2.69	7.62	13.71

In the process of grouting and plugging the magnetic self-polymerization slurry, the first shear failure is often at the inner wall of the pipeline, where the magnetic adsorption has a minor influence, and the shear strength is the weakest. The above derivation formula can be used to calculate the shear strength of magnetic self-agglomerating grout with different plugging lengths and different magnetic field distances, which provides an important theoretical reference for underground engineering management.

5. Conclusions

This paper takes the pipeline water burst in the karst area as the research object. WEMS was developed, and the orthogonal test of magnetic self-polymerization slurry plugging was carried out using the self-developed visual karst pipeline water burst grouting plugging simulation test system. Finally, the shear mechanism of magnetic slurry magnetization plugging was analyzed. The specific conclusions of this study are as follows:

(1) Experiments show that when the water–cement ratio of the new WEMS is 0.35–0.55 and the amount of Fe_3O_4 powder is 20–40%, the grouting sealing performance is the best.
(2) The orthogonal test was carried out on the plugging law of the magnetic self-polymerizing slurry under high flow velocity and dynamic water conditions. The water plugging pressure, dynamic water flow rate, and slurry retention rate were selected as evaluation indexes, and the primary and secondary relationships of the influencing factors of each evaluation index were obtained by range analysis.
(3) In the indoor experiment, the primary and secondary relationship between various factors and slurry plugging pressure was determined as plugging length > Fe_3O_4 power ratio > water–cement ratio. The water plugging pressure is positively correlated with the length of water plugging and the amount of Fe_3O_4 powder, and the water plugging pressure increases with its increase.
(4) In the analysis of the dynamic water flow rate and the dynamic water anti-scouring effect, the dynamic water flow rate and slurry retention rate are most affected by the amount of Fe_3O_4 powder, followed by the plugging length, and the water–cement ratio has a minor effect. The new WEMS can effectively complete the long-distance plugging of karst pipelines.
(5) The relationship between the shear strength and magnetic field strength, plugging length, and slurry ratio was established by analyzing the force of WEMS in the process of grouting plugging.

Author Contributions: Introduction, J.L. and S.L.; materials and methods, J.L. and S.L.; results, B.P. and M.W.; discussion and conclusions, S.L.; writing—original draft, S.L. and M.W. All authors have read and agreed to the published version of the manuscript.

Funding: The authors gratefully acknowledge the financial support provided by the National Natural Science Foundation of China (52079071), the Natural Science Research Project of Yichang (A22-3-003), the Fund for the Opening of key Laboratory of Geological Disaster in the Three Gorges Reservoir Area by the Ministry of Education (2020KDZ08) and the Research Fund for Excellent Dissertation of China Three Gorges University (2021BSPY016).

Institutional Review Board Statement: Not applicable.

Informed Consent Statement: Not applicable.

Data Availability Statement: The research data are included within the article, and further data are available from the first and corresponding author upon request.

Conflicts of Interest: The authors declare no conflicts of interest.

References

1. Li, S.C.; Xu, Z.H.; Huang, X.; Lin, P.; Zhao, X.C.; Zhang, Q.S.; Yang, L.; Zhang, X.; Sun, H.F.; Pan, D.D. Classification, geological identification, hazard mode and typical case studies of hazard-causing structures for water and mud inrush in tunnels. *Chin. J. Rock Mech. Eng.* **2018**, *37*, 1041–1069. (In Chinese)
2. Xu, Z.; Lin, P.; Xing, H.; Pan, D.; Huang, X. Hydro-mechanical coupling response behaviors in tunnel subjected to a water-filled karst cave. *Rock Mech. Rock Eng.* **2021**, *54*, 3737–3756. [CrossRef]
3. Xu, Z.H.; Wang, W.Y.; Lin, P.; Nie, L.C.; Wu, J.; Li, Z.M. Hard-rock TBM jamming subject to adverse geological conditions: Influencing factor, hazard mode and a case study of Gaoligongshan Tunnel. *Tunn. Undergr. Space Technol.* **2021**, *108*, 103683. [CrossRef]
4. Lin, P.; Xiong, Y.; Xu, Z.; Wang, W.; Shao, R. Risk assessment of TBM jamming based on Bayesian networks. *Bull. Eng. Geol. Environ.* **2022**, *81*, 47. [CrossRef]
5. Jin, Q.; Bu, Z.; Pan, D.; Li, H.; Li, Z.; Zhang, Y. An integrated evaluation method for the grouting effect in karst areas. *KSCE J. Civ. Eng.* **2021**, *25*, 3186–3197. [CrossRef]
6. Xu, Z.; Bu, Z.; Pan, D.; Li, D.; Zhang, Y. A novel numerical method for grouting simulation in flowing water considering uneven spatial and temporal distribution of slurry: Two-Fluid Tracking (TFT) method. *Comput. Geotech.* **2022**, *147*, 104756. [CrossRef]
7. Wang, F.T.; Zhang, C.; Wei, S.F.; Zhang, X.G.; Guo, S.H. Whole section anchor-grouting reinforcement technology and its application in underground roadways with loose and fractured surrounding rock. *Tunn. Undergr. Space Technol.* **2016**, *51*, 133–143.
8. Li, P.; Zhang, Q.; Zhang, X.; Li, S.; Li, X.; Zuo, J. Grouting diffusion characteristics in faults considering the interaction of multiple grouting. *Int. J. Geomech.* **2017**, *17*, 04016117. [CrossRef]
9. Sha, F.; Lin, C.; Li, Z.; Liu, R. Reinforcement simulation of water-rich and broken rock with Portland cement-based grout. *Constr. Build. Mater.* **2019**, *221*, 292–300. [CrossRef]
10. Feng, Z.; Kang, H.; Yang, J. Discussion on grouting technology for crack rock mass. *Coal Sci. Technol.* **2005**, *33*, 63–66.
11. Ruan, W.; Wang, W.; Hu, A. Development and application of new kind of cement composite grout. *Chin. J. Geotech. Eng.* **2001**, *23*, 212–216.
12. Ge, J. Development and prospect of chemical grouting techniques. *Chin. J. Rock Mech. Eng.* **2006**, *25* (Suppl. S2), 3384–3392.
13. Bezuijen, A.; Grotenhuis, T.; Vantol, A.F. Analytical model for fracture grouting in sand. *J. Geotech. Geoenviron. Eng.* **2010**, *137*, 611–620. [CrossRef]
14. Sui, W.H.; Liu, J.Y.; Hu, W.; Qi, J.F.; Zhan, K.Y. Experimental investigation on sealing efficiency of chemical grouting in rock fracture with flowing water. *Tunn. Undergr. Space Technol.* **2015**, *50*, 239–249. [CrossRef]
15. Xu, Z.P.; Liu, C.W.; Zhou, X.W. Full-scale physical modelling of fissure grouting in deep underground rocks. *Tunn. Undergr. Space Technol.* **2019**, *89*, 249–261. [CrossRef]
16. Xiao, F.; Zhao, Z.Y.; Chen, H.M. A simplified model for predicting slurry flow in fracture channels. *Tunn. Undergr. Space Technol.* **2017**, *70*, 11–18. [CrossRef]
17. Huang, H.; Rong, Y. Saturated sand layer water flooding seepage grouting analysis. *Geotech. Mech.* **2009**, *30*, 2016–2020.
18. Yang, X.; Lei, J.; Xia, L. Study on diffusion radius of power-law grout. *Geomechanics* **2005**, *26*, 1803–1806.
19. Zhan, K.; Sui, W.; Gao, Y. Single fracture hydrodynamic grouting diffusion model. *Geomechanics* **2011**, *32*, 1659–1663.
20. Zhan, J.; Sui, W.; Wang, W. Correlation analysis between seepage pressure and water plugging effect of fracture grouting. *Geotech. Mech.* **2012**, *33*, 2650–2655.
21. Li, S.; Zhang, X.; Zhang, Q. Study on diffusion mechanism and sealing method of grouting water-stop slurry for water inrush in underground engineering. *J. Rock Mech. Eng.* **2011**, *30*, 2377–2395.
22. Rabinow, J. The magnetic fluid clutch. *Electr. Eng.* **1951**, *67*, 1167. [CrossRef]
23. Li, L.; Guan, J.; Cheng, H. Preparation of polyethylene glycol coated carbonyl iron core-shell particles and properties of water-based magnetorheological fluid. *J. Phys. Chem.* **2005**, *21*, 817–821.
24. Carlson, J.D. Properties and Applications of Commercial Magnetorheological Fluids. *J. Intell. Mater. Syst. Struct.* **1998**, *10*, 5–13.
25. Lim, S.H.; Prusty, B.G.; Pearce, G.; Kelly, D.; Thomson, R.S. Study of magnetorheological fluids towards smart energy absorption of composite structures for crashworthiness. *Mech. Adv. Mater. Struct.* **2016**, *23*, 538–544. [CrossRef]
26. Xu, Z.D.; Shen, Y.P.; Guo, Y.Q. Semi-active control of structures incorporated with magnetorheological dampers using neural networks. *Smart Mater. Struct.* **2003**, *12*, 80–87.
27. Ghorbani, S.; Sharifi, S.; Rokhsarpour, H.; Shoja, S.; Gholizadeh, M.; Rahmatabad, M.A.D.; de Brito, J. Effect of magnetized mixing water on the fresh and hardened state properties of steel fibre reinforced self-compacting concrete. *Construct. Build. Mater.* **2020**, *248*, 118660. [CrossRef]
28. Ku, T.; Palanidoss, S.; Zhang, Y.; Moon, S.W.; Wei, X.; Huang, E.S.; Kumarasamy, J.; Goh, K.H. Practical configured microtremor array measurements (MAMs) for the geological investigation of underground space. *Undergr. Space* **2020**, *6*, 240–251. [CrossRef]

29. Mu, R.; Zhao, Q.; Tian, W. Preparation and properties of unidirectional steel fiber reinforced cement slurry. *J. Hebei Univ. Technol.* **2012**, *41*, 101–104.
30. Song, H.; Ding, Y. Review on the research methods of spatial distribution of steel fibers in concrete matrix. *J. Mater. Sci. Eng.* **2015**, *33*, 768–775.
31. Li, Y.; Yi, S.; Zhang, L.; Xu, R. Research status and development prospect of magnetized water cement concrete. *J. Mater. Sci. Eng.* **2019**, *37*, 331–338.
32. Zhao, H.; Dai, X.; Zeng, X.; Liu, Y. Experimental Study on Reducing Dust Content of Shotcrete by Magnetized Water. *J. Min. Saf. Eng.* **2008**, *03*, 371–374.
33. Liu, F.; Cai, X. Study on the sealing scheme of annular magnet pressure bonding for large diameter pipeline. *New Technol. New Process* **2012**, *08*, 39–41.
34. Liu, J.; Guo, J.; Yu, F.; Li, Z. Experimental Study on Reinforcement of Reef Limestone by Magnetic Anchoring System. *Materials* **2023**, *16*, 3519. [CrossRef]
35. *DL/T5126-2001*; Test Code on Polymer-Modified Cement Martor. National Standard of China: Beijing, China, 2001.

Disclaimer/Publisher's Note: The statements, opinions and data contained in all publications are solely those of the individual author(s) and contributor(s) and not of MDPI and/or the editor(s). MDPI and/or the editor(s) disclaim responsibility for any injury to people or property resulting from any ideas, methods, instructions or products referred to in the content.